AGU PUBLICATIONS

Geophysical Research Letters

RESEARCH LETTER
10.1002/2016GL071263

Key Points:
- Rupture history of the 2016 Amatrice (Italy) normal faulting earthquake
- Rupture directivity affecting damage pattern during the ML 6.0, 2016, Amatrice (Italy) earthquake
- Slip heterogeneity characterizing moderate-magnitude normal faulting earthquakes in the Apennines

Correspondence to:
E. Tinti,
elisa.tinti@ingv.it

Citation:
Tinti, E., L. Scognamiglio, A. Michelini, and M. Cocco (2016), Slip heterogeneity and directivity of the M_L 6.0, 2016, Amatrice earthquake estimated with rapid finite-fault inversion, *Geophys. Res. Lett.*, *43*, 10,745–10,752, doi:10.1002/2016GL071263.

Received 19 SEP 2016
Accepted 14 OCT 2016
Accepted article online 15 OCT 2016
Published online 30 OCT 2016

Slip heterogeneity and directivity of the M_L 6.0, 2016, Amatrice earthquake estimated with rapid finite-fault inversion

E. Tinti[1], L. Scognamiglio[1], A. Michelini[1], and M. Cocco[1]

[1]Istituto Nazionale di Geofisica e Vulcanologia, Rome, Italy

Abstract On 24 August 2016 a magnitude M_L 6.0 occurred in the Central Apennines (Italy) between Amatrice and Norcia causing nearly 300 fatalities. The main shock ruptured a NNW-SSE striking, WSW dipping normal fault. We invert waveforms from 26 three-component strong motion accelerometers, filtered between 0.02 and 0.5 Hz, within 45 km from the fault. The inferred slip distribution is heterogeneous and characterized by two shallow slip patches updip and NW from the hypocenter, respectively. The rupture history shows bilateral propagation and a relatively high rupture velocity (3.1 km/s). The imaged rupture history produced evident directivity effects both N-NW and SE of the hypocenter, explaining near-source peak ground motions. Fault dimensions and peak slip values are large for a moderate-magnitude earthquake. The retrieved rupture model fits the recorded ground velocities up to 1 Hz, corroborating the effects of rupture directivity and slip heterogeneity on ground shaking and damage pattern.

1. Introduction

On 24 August 2016, at 01:36:32 UTC a M_L 6.0 earthquake hit a portion of the Central Apennines (Italy) between Norcia and Amatrice towns, devastating the latter one, Accumoli and several surrounding small towns, killing almost 300 people. The hypocenter is located at 42.70°N, 13.23°E at the depth of 8 km (http://cnt.rm.ingv.it/event/7073641). The moment tensor solution, immediately released by INGV, shows normal faulting with planes striking along the Apenninic direction, and a scalar seismic moment equal to 1.07×10^{18} Nm (M_w 6.0) (http://cnt.rm.ingv.it/event/7073641/?tab=MeccanismoFocale-TDMTinfo). At the moment, the largest aftershock (M_L 5.4) occurred almost 1 h after the main shock, it is located 12 km NW of the main shock close to the Norcia town and it also features a normal faulting moment tensor solution similar to most of the aftershocks ($M_L > 3.0$) (http://cnt.rm.ingv.it/event/7076161/?tab=MeccanismoFocale-TDMTinfo). No foreshocks were recorded and identified. The epicentral area is one of the regions with the highest seismic hazard in Italy characterized by a 10% probability of exceedance in 50 years of horizontal PGA value of 0.250–0.275 g [*Stucchi et al.*, 2011].

This sector of the Central Apennines is characterized by two major NNW-SSE trending extensional fault systems of adjacent, west dipping, active Quaternary faults (Figure 1). The western faults alignment runs from Gubbio to Colfiorito, Norcia, and L'Aquila. The eastern system develops from Mount Vettore to Amatrice-Campotosto (Mount Gorzano fault) and Gran Sasso ridge [*Boncio et al.*, 2004; *Galadini and Galli*, 2000; *Lavecchia et al.*, 2012, and references therein]. While the western system is certainly seismogenic as indicated by the earthquakes that recently occurred on some of these structures (Gubbio 1984, M_w 5.6; Colfiorito 1997, M_w 6.0; Norcia 1979, M_w 5.9; and L'Aquila 2009, M_w 6.1), the seismogenic behavior of the eastern fault system has been largely debated mainly in the geological community [*Boncio et al.*, 2004; *Galadini et al.*, 1999; *Galadini and Galli*, 2000; *Lavecchia et al.*, 2012]. The Mount Vettore and Gran Sasso faults seem to have been silent since historical times [*Boncio et al.*, 2004]. The northern portion of the Gorzano fault has not been active in instrumental times but could be the source of the only large historical earthquake reported in this area: the 7 October 1639 (I = IX-X MCS, M = 6.2, CPTI15, Figure 1) [*Rovida et al.*, 2016]. The southern part, which did not show historical destructive events, was activated during the L'Aquila 2009 sequence [*Lavecchia et al.*, 2012; *Chiaraluce*, 2012]. The extensional active fault systems are often segmented by tectonic structures inherited from past compressional tectonics. Understanding the main features of the Amatrice seismic source contributes to explain the seismogenic processes in the Central Apennines.

Current advances in data transmission and communication yield high-quality broadband and strong-motion waveforms in near real time that are fundamental for rapid determination of earthquake focal mechanisms

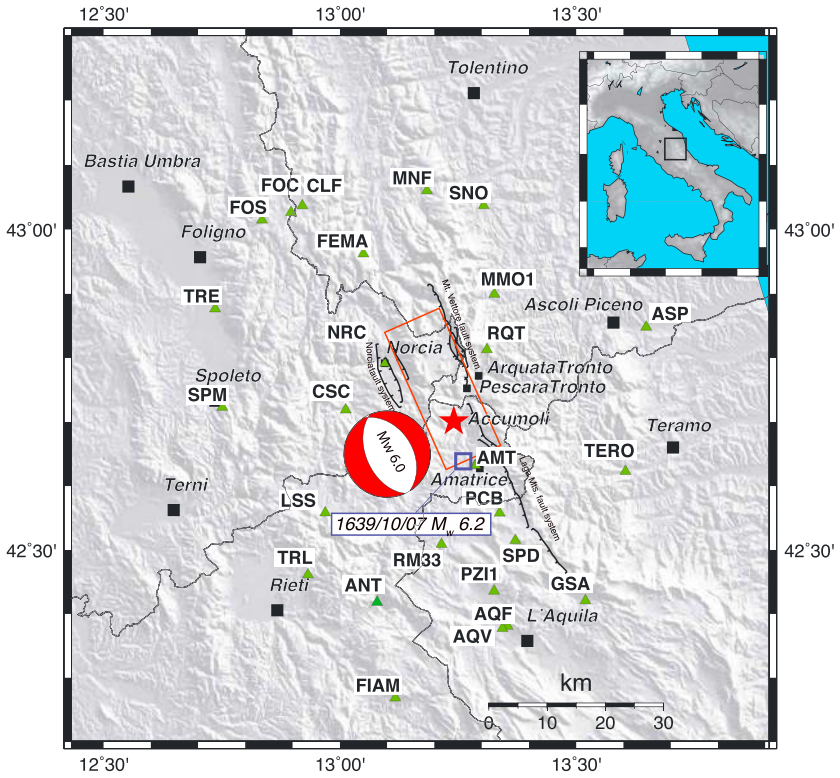

Figure 1. Distribution of the strong motion stations (green triangles) used to retrieve the slip model of the 2016 Amatrice main shock. Traces of the active faults [*EMERGEO Working Group*, 2016] and the time domain moment tensor (TDMT) solution are also shown. The red rectangle represents the surface projection of the fault plane adopted in this study. The red star is the epicenter location released by INGV. The blue square indicates the location of the largest historical earthquake that occurred in this area (October 1639, I = IX-X MCS, M = 6.2).

and fast finite-fault rupture modeling. Only a few hours after the event, the strong motion recordings were released by INGV [*Amato and Mele*, 2008] and RAN (http://ran.protezionecivile.it/IT/index.php) seismic networks making it possible to start the kinematic modeling to image the earthquake coseismic rupture providing the first preliminary models within 48 h of the main shock.

In this study, we present a first kinematic model of the 2016 Amatrice earthquake obtained using the (near-real-time) procedure proposed by *Dreger and Kaverina* [2000] to invert strong motion data. Our results provide some basic constraints to the rupture history of this earthquake, allowing a preliminary interpretation of the aftershock sequence and elements to appraise and better contextualize the observed ground shaking.

2. Data

We have inverted the recordings of the 26 three-component digital accelerometers of the RAN and INGV networks closest to the epicenter (Figure 1). The epicentral distances of the selected recording sites are less than ~45 km. The recorded accelerograms were processed to remove the mean offset and instrument response, band-pass filtered between 0.02 and 0.5 Hz using a low-pass filter with three poles and a high-pass filter with three poles, and finally integrated in time to obtain ground velocities. The maximum frequency of 0.5 Hz was also selected to reduce the possible contributions of local site effects [*Bindi et al.*, 2011] onto the source inversion modeling. The processed time histories were then resampled at 10 samples per second. The 26 inverted stations have different elevations that, except ASP and TRE stations (89 and 261 m above sea level, respectively, see Figure 1), range between ~560 and ~1340 m. Because of the significant topography of the area, we determined the average elevation of the inverted stations (~850 m) and in the following all depth values refer to this average altitude. This is necessary to account for the topography of the Apennine belt and facilitate the comparison with SAR (Synthetic Aperture Radar) modeling.

3. Inversion Methodology

The inversion code is based on the method of *Hartzell and Heaton* [1983], as implemented by *Dreger and Kaverina* [2000] and *Dreger et al*. [2005] and consists of a nonnegative, least squares inversion method with simultaneous smoothing and damping.

The main objective of a fast finite-fault kinematic inversion consists of imaging the main features of the earthquake rupture history in terms of heterogeneous distribution of slip amplitudes, slip direction, and average rupture velocity [*Scognamiglio et al*., 2010; *Dreger and Kaverina*, 2000]. This approach assumes a constant rupture velocity and allows us to use multiple time windows to account for potential variations in rupture speed and local rise time. It follows that the best fitting slip duration and rupture velocity in each time window have been selected iteratively by performing inversions with different values of these parameters and quantitatively measuring the fit based on a variance reduction, as defined in *Dreger et al*. [2005]. The local slip velocity is modeled by imposing a simple boxcar source-time function. Although some of the assumptions above are very simplistic, they have been found generally effective to perform rapid preliminary inversions of the recorded seismograms [*Scognamiglio et al*., 2010]. The Green's functions were computed using a FORTRAN, frequency wave number integration program [*Saikia*, 1994; *Wang and Herrmann*, 1980]. We adopt the precalculated and stored Green's functions obtained using the CIA (Central Italian Apennines) velocity model [*Herrmann et al*., 2011]. This model has been inferred for the Central Apennines during the 2009 L'Aquila sequence. The Green's functions are computed on a regular grid sampling the focal volume every 1 km horizontally and 1 km vertically and filtered between 0.02 and 0.5 Hz, the same as for the recorded data.

4. Fault Parameterization

The analysis of geodetic data (GPS and SAR observations) allows for the identification of the fault plane between the two nodal planes of the time domain moment tensor (TDMT) focal mechanism [*Gruppo di lavoro IREA-CNR & INGV*, 2016]. In particular, interferometric images show that the deformation pattern is consistent with the southwestern dipping nodal plane of the moment tensor solution. For this reason, in this work, we have assumed a fault plane striking 156° and dipping 50° to the SW. We have tested different hypocentral depths (4–10 km) and different fault dimensions. The adopted fault dimension is 26 km long and 16 km width. The chosen fault extension is corroborated by the GPS displacement vectors at Amatrice and Norcia; the recorded horizontal displacements at AMT and NRC suggest the causative fault to terminate before the Amatrice town to the SE and to extend as far as Norcia to the NW [*INGV Working Group "GPS Geodesy, GPS data and data analysis center"*, 2016].

During the inversion we allowed rise time and rupture velocity to range between 0.3 and 2.5 s, and 2.5 and 4.0 km/s, respectively. The rake was allowed to be heterogeneous throughout the fault ranging between −45° and −125°, that is, ±40° relative to the TDMT slip direction. The fault was parameterized using 104 subfaults each having a $2 \times 2\,km^2$ area.

5. Results

We determined the kinematic finite-fault model by imposing both single-window and multiwindow models of fault rupture. The best solutions that maximize the variance reduction have in both cases very similar slip distributions and kinematic parameters. In Figure 2, we show the best fitting rupture model inferred from the multiwindow inversion of ground velocity time histories. It is obtained after selecting the hypocentral depth of 7.3 km (corresponding to a 6.45 km depth below sea level). The fault top reaches 0.4 km depth (0.45 km above sea level). This model has a constant rise time of 1.2 s given by three windows of 0.4 s each. The best rupture velocity of each window is 3.1 km/s. The total inferred seismic moment is 1.6×10^{18} Nm corresponding to a M_w 6.1 (similar to the M_w 6.0 inferred by TMDT solution, http://cnt.rm.ingv.it/tdmt).

The most relevant features of this model are (i) bilateral rupture, (ii) relatively fast rupture velocity (3.1 km/s), (iii) heterogeneity of the slip distribution characterized by two main slip patches, and (iv) quite different value of the rake on the two patches. The southeastern slip patch (4 km updip from the hypocenter) has a relatively large maximum slip (99 cm). The northwestern slip patch is located ~10 km from the hypocenter at a similar depth ~4.2 km, corresponding to ~5.5 km along dip as shown in Figure 2, and it has a larger rupture area and

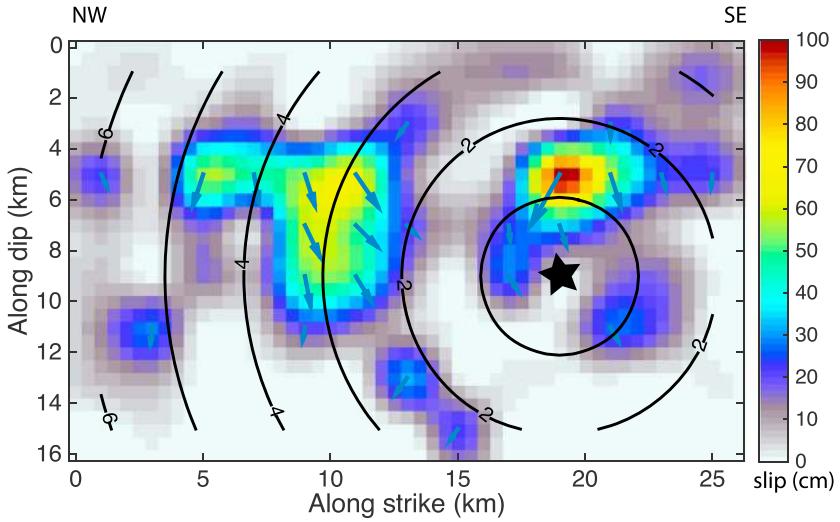

Figure 2. Rupture model imaged in this study by inverting ground velocity time histories. Slip amplitudes are expressed in centimeters and rupture times in seconds, as shown by contour lines. The inferred rupture velocity is $V_r = 3.1$ km/s. The blue arrows indicate the slip direction for slip larger than 20 cm.

an average mean slip of ~55 cm. The patch updip from the hypocenter has a rake close to −120°, while the patch northwest from the hypocenter has a rake close to −70°.

The synthetic seismograms match the recorded ground velocities particularly well, and the variance reduction is 60% (Figure 3). Our results suggest that the main slip patch rupturing between 1 and 2 s updip

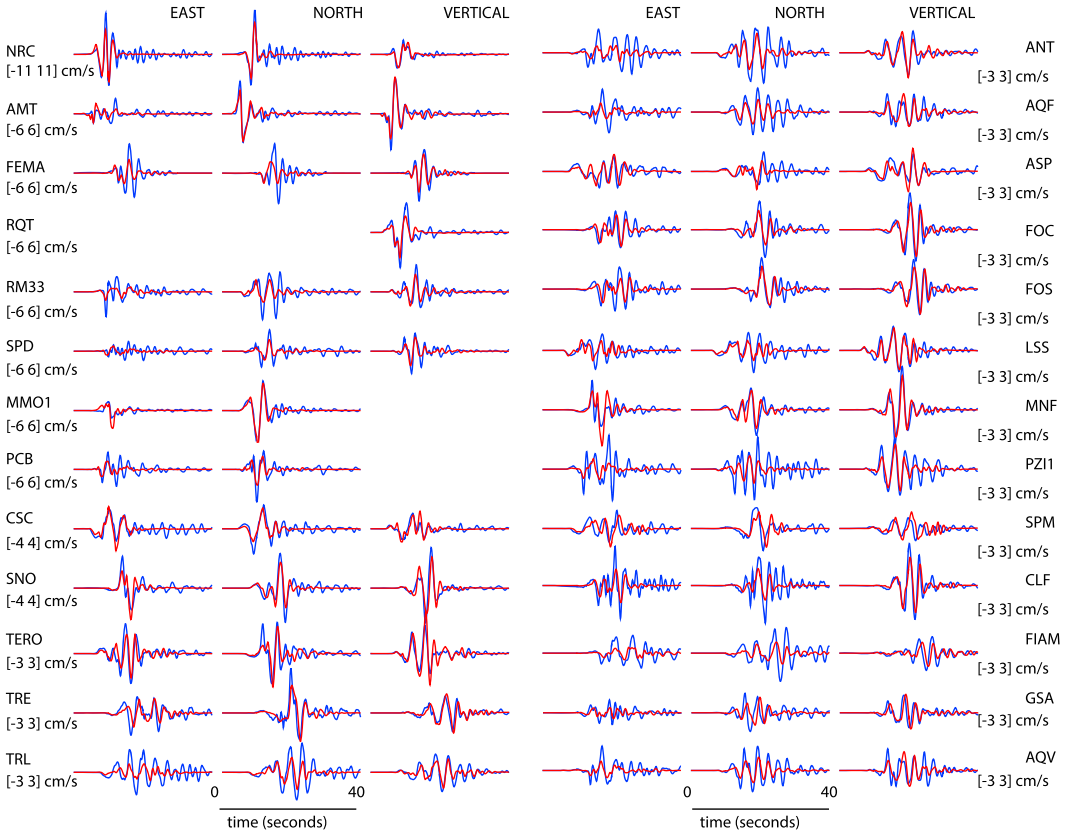

Figure 3. Fit to the data: synthetic ground velocity filtered between 0.02 and 0.5 Hz (red lines) and recorded strong motions (blue lines). Numbers in brackets represent the amplitude range in cm/s for each station.

from the hypocenter and toward SE is required to fit the ground motion time histories recorded at the closest stations to the SE of the hypocenter (i.e., AMT, PCB, TERO, RM33, and SPD). The patch rupturing between 2 and 5 s northwest from the hypocenter explains the high values of PGV recorded at the Norcia station and at the other stations northwestward [*INGV-ReLUIS Working Group*, 2016].

Noteworthy, the best fitting model requires two slip patches with different rake angles. This result suggests that the rupture could have occurred either on a single fault with two very different slip directions or perhaps most likely on two different planes featuring minor differences in strike and dip angles but with more similar rake angles. These fault segments could be related to the previously mentioned normal faults systems of Mount Vettore and Mount Gorzano (Figure 4) [*Boncio et al*., 2004; *Galadini and Galli*, 2000; *Barchi et al*., 2000; *Lavecchia et al*., 2012]. The lack of aftershocks in the southeastern fault segment between Accumoli and Amatrice (Figure 4) is consistent with the location of the main slip patch updip of the hypocenter. The aftershocks clustering near Amatrice is consistent with the termination of the modeled main shock causative fault and might be associated with a portion of the Mount Gorzano fault. The aftershock pattern to the northwest of the hypocenter, between Accumoli and Norcia, is more sparse, suggesting a complex fault system with antithetic faults activated by aftershocks, and it is consistent with the location of the second slip patch near Norcia.

Despite the moderate magnitude of the main shock, the retrieved rupture history displays a remarkable heterogeneous slip distribution on a relatively large fault dimension with two main patches featuring high peak slip values.

The imaged rupture history is consistent with the observed directivity focusing seismic energy mainly toward the N-NW as well as toward Amatrice town and nearby villages to the SE in agreement with the pulses recorded by the strong motion data [*INGV-ReLUIS Working Group*, 2016] and the preliminary reports from the damaged area [*Gruppo di Lavoro INGV sul terremoto di Amatrice*, 2016].

6. Discussion and Conclusion

The near-real-time availability of high-quality geodetic and seismological data immediately after the Amatrice main shock allowed for the constraining of the causative fault geometry and the modeling of the rupture history through the fast finite-fault inversion procedure implemented at INGV [*Scognamiglio et al*., 2010]. Less than 48 h after the main shock, we determined an initial reliable rupture history of the main shock that, with minor adjustments, is that presented in this paper (Figure 2). Overall, our results show that the rupture history of the Amatrice earthquake features a heterogeneous slip distribution with high peak slip values and a relatively high rupture velocity. Slip is concentrated mainly on two patches: the first one located updip from the hypocenter and the second northwestward along the strike direction. Both slip patches are shallower than the hypocentral depth, with the second patch extending at depth downdip. The proposed model fits well the available ground velocities recorded at the closest stations (Figure 3). The inferred bilateral rupture and the rupture history can explain the observed directivity effects, both those toward N-NW and those updip and toward SE and Amatrice.

In order to assess quantitatively the source contribution to the ground shaking observed at the closest recording stations, we have performed a forward modeling of predicted ground motion time histories up to 1 Hz. We are aware that extending the frequency range for forward modeling would have required taking into account site effects. Therefore, assessing the source contribution to ground motion time histories up to 1 Hz does not exclude the role of site amplifications on ground shaking and local damage patterns locally. In Figure 4 we show the surface projection of the slip described in Figure 2 and the match between synthetics and real data for the three closest stations (Norcia, Arquata del Tronto, and Amatrice) for two different frequency ranges (0.02–0.5 and 0.02–1.0 Hz). In summary, we have computed synthetic ground velocities through forward modeling in the frequency bandwidth 0.02–1.0 Hz by using the best fitting source model (shown in Figure 2) obtained from the inversion of ground velocity time histories in the low-frequency bandwidth 0.02–0.5 Hz. To facilitate the comparison, we show in Figure 4 the fit to the data for both frequency ranges. We note that the kinematic model imaged at lower frequencies is able to match well also the prominent pulse observed along the NS and vertical components of the Amatrice station (AMT) at higher frequencies (1 Hz). The match between recorded and calculated ground motion is indeed quite remarkable given that we expect the high-frequency signal being more affected by local site effects. To this regard, *Bindi et al*. [2011] reported strong local site amplifications in the Norcia basin using a seismic station temporarily

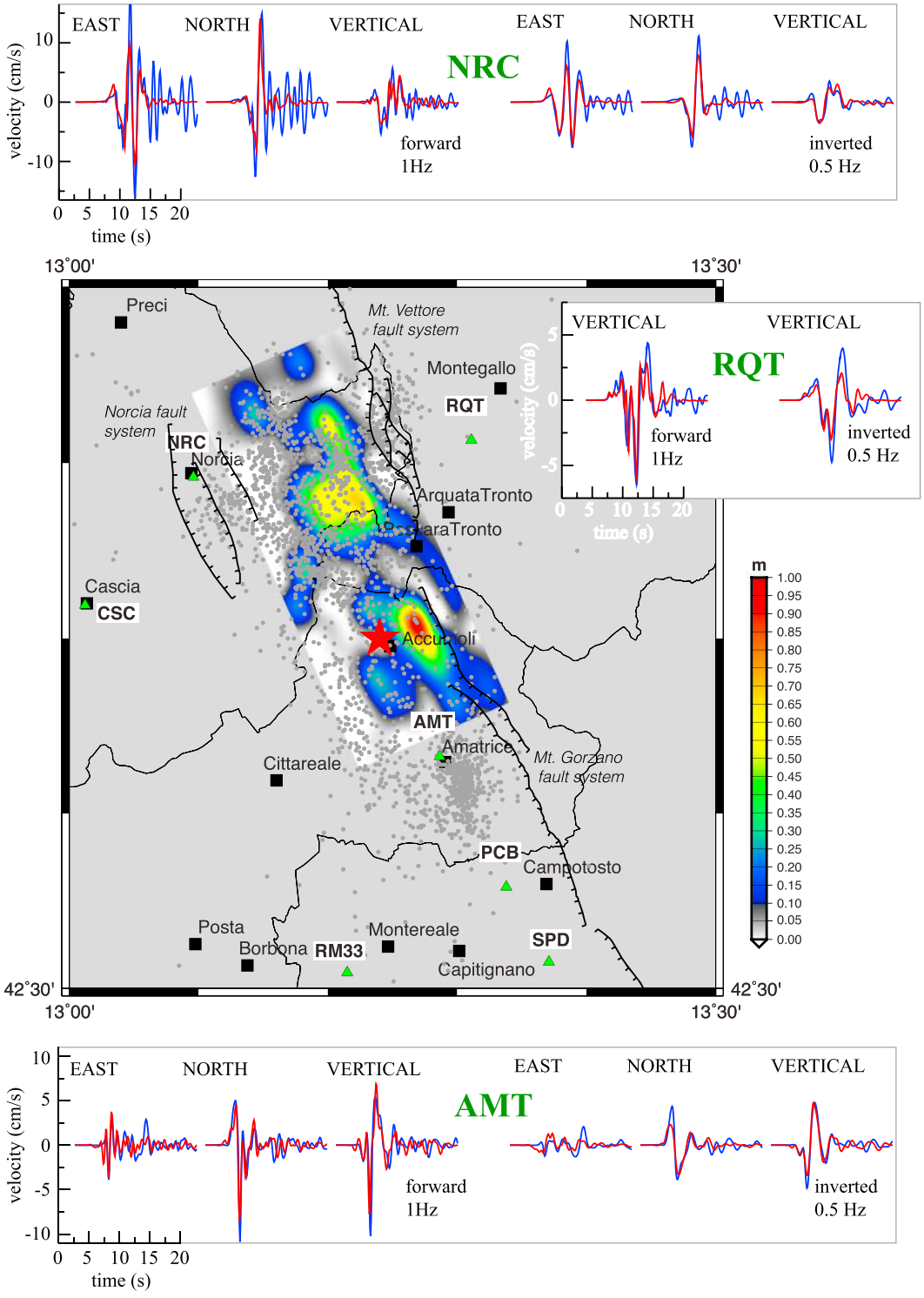

Figure 4. Surface projection of the inverted slip distribution. Gray dots display the locations of the early aftershocks (5 days after the main shock) downloaded from EIDA portal (eida.rm.ingv.it). Fit between synthetics (red lines) and real data (blue lines) for the three closest stations (NRC, Norcia; RQT, Arquata del Tronto; and AMT, Amatrice) in two different frequency ranges: [0.02–0.5 Hz] and [0.02–1.0 Hz]. Synthetic waveforms up to 0.5 Hz are obtained from the performed inversion, while synthetics up to 1 Hz are forward modeled using the source model retrieved from the inversion up to 0.5 Hz.

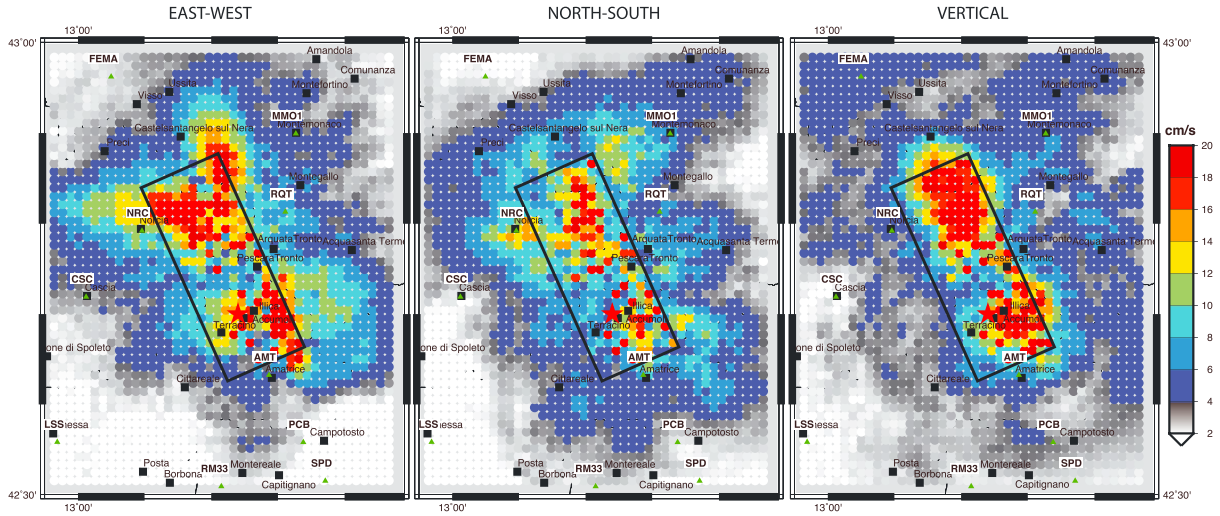

Figure 5. Map of peak ground velocity (PGV) for the horizontal and vertical components computed from forward modeling of synthetics seismograms up to 1 Hz for a dense grid of phantom receivers spaced at 1 km.

deployed at about 100 m from NRC (class B of EC8); they found evident site amplifications in the frequency range 1.5–3 Hz for the vertical and over 0.7–3 Hz for the EW component. We also note that most receivers used in our modeling attempt have been assigned to class B* of EC8, which are expected to be relatively free for local amplifications.

In Figure 5, we plot the PGV for horizontal and vertical components retrieved by computing synthetics seismograms up to 1 Hz for a dense grid of phantom receivers. This figure shows that slip heterogeneity and rupture directivity alone can explain the reported variability of ground shaking in the near source, and they are likely key factors for the increased intensity level reported in numerous villages located near the fault such as Accumoli, Arquata del Tronto, and Amatrice. The smaller PGV values predicted to the south and southwest of Amatrice agree well with the reduced reported macroseismic intensities. In addition, the pattern of the simulated PGV values appears to be compatible with the intensity levels in the area NE of the fault plane [*INGV-ReLUIS Working Group*, 2016]. These observations let us to deduce that the rupture directivity and the source heterogeneity contributed to the damages observed in the epicentral area. This does not exclude that site effects might have accentuated locally the amplitude of the ground shaking.

The ground velocity recorded at Amatrice displays a relatively simple time history characterized by evident pulses at nearly 0.5 Hz (see Figures 3 and 4) on the NS and vertical components. We interpret this peculiar polarization of the recorded waveforms as the effect of the breakage of an asperity (high-stress drop and high slip) near the hypocenter and the consequent rupture propagation, likely at a nearly constant speed, which focused radiated energy in a narrow frequency (around 2 s) bandwidth and generated a relatively coherent ground velocity signal. This might have contributed to explain the heavy damages in Amatrice increasing the already high vulnerability of buildings. This observation further corroborates the different ways to interpret source directivity in the near field.

Acknowledgments

We are very grateful to the Editor Andrew V. Newman and Michel Bouchon and an anonymous reviewer for comments and suggestions that significantly improved the manuscript. We would like to thank Doug Dreger for providing us the latest version of the finite-fault inversion code and Sandro Marcucci and the RAN team, Lucia Luzi, Marco Cattaneo, Giancarlo Monachesi, and the INGV National Seismic Network team for providing us the strong motion data. We thank Stefano Pucci, Paolo Marco Martini, Fabio Villani, Giuseppe Pezzo, Stefano Salvi, Daniele Cheloni, Antonio Avallone, Emanuele Casarotti, GdL GPS-INGV, GdL SAR-INGV, and GdL INGV-DPC for helpful discussions and for sharing preliminary results of their investigations. We have appreciated and benefited of the work and discussions during the meeting of the "INGV Emergency Unit," which was able to elaborate a first preliminary interpretative report after 48 h from the main shock to be delivered to Italian Civil Protection. Some figures were made using the Generic Mapping Tools version 4.2.1 (http://gmt.soest.hawaii.edu). Data used in this article are available at the ESM-Engineering Strong-Motion database (http://esm.mi.ingv.it/). Laura Scognamiglio is founded by the INGV-DPC (2012–2021) agreement (All. A -Cap. 3.1.01.11).

References

Amato, A., and F. Mele (2008), Performance of the INGV National Seismic Network from 1997 to 2007, *Ann. Geophys.*, *51*(2-3), 417–431, doi:10.4401/ag-4454.

Barchi, M., F. Galadini, G. Lavecchia, P. Messina, A. M. Michetti, L. Peruzza, A. Pizzi, E. Tondi, and E. Vittori (Eds) (2000), *Sintesi delle Conoscenze sulle Faglie Attive in Italia Centrale: Parametrizzazione ai Fini della Carattrizzazione della Pericolosità Sismica*, pp. 62 , CNR-GNDT, Rome.

Bindi, D., L. Luzi, S. Parolai, D. Di Giacomo, and G. Monachesi (2011), Site effects observed in alluvial basins: The case of Norcia (Central Italy), *Bull. Earthquake Eng.*, *9*(6), 1941–1959, doi:10.1007/s10518-011-9273-3.

Boncio, P., G. Lavecchia, G. Milana, and B. Rozzi (2004), Seismogenesis in Central Apennines, Italy: An integrated analysis of minor earthquake sequences and structural data in the Amatrice-Campotosto area, *Ann. Geophys.*, *47*(6), 1723–1742.

Chiaraluce, L. (2012), Unravelling the complexity of Apenninic extensional fault systems: A review of the 2009 L'Aquila earthquake (Central Apennines, Italy), *J. Struct. Geol.*, *42*, 2–18.

Dreger, D. S., and A. Kaverina (2000), Seismic remote sensing for the earthquake source process and near-source strong shaking: A case study of the October 16, 1999 Hector Mine earthquake, *Geophys. Res. Lett.*, *27*(13), 1941–1944, doi:10.1029/1999GL011245.

Dreger, D. S., L. Gee, P. Lombard, M. H. Murray, and B. Romanowicz (2005), Rapid finite-source analysis and near-fault strong ground motions: Application to the 2003 M_w 6.5 San Simeon and 2004 M_w 6.0 Parkfield earthquakes, *Seismol. Res. Lett.*, *76*(1), 40–48.

EMERGEO Working Group (2016), The 24 August 2016 Amatrice earthquake: Coseismic Effects, doi:10.5281/zenodo.61568.

Galadini, F., and P. Galli (2000), Active tectonics in the Central Apennines (Italy)—Input data for Seismic Hazard Assessment, *Nat. Hazards*, *22*, 225–270.

Galadini, F., P. Galli, I. Leschiutta, G. Monachesi, and M. Stucchi (1999), Active tectonics and seismicity in the area of the 1997 earthquake sequence in Central Italy: A short review, *J. Seismol.*, *3*, 165–175.

Gruppo di Lavoro INGV sul terremoto di Amatrice (2016), Secondo rapporto di sintesi sul Terremoto di Amatrice Ml 6.0 del 24 Agosto 2016 (Italia Centrale), doi:10.5281/zenodo.154400.

Gruppo di lavoro IREA-CNR & INGV (2016), Sequenza sismica di Amatrice: Aggiornamento delle analisi interferometriche satellitari e modelli di sorgente, doi:10.5281/zenodo.61682.

Hartzell, S. H., and T. H. Heaton (1983), Inversion of strong ground motion and teleseismic waveform data for the fault rupture history of the 1979 Imperial Valley, California, earthquake, *Bull. Seismol. Soc. Am*, *73*(6), 1553–1583.

Herrmann, R. B., L. Malagnini, and I. Munafò (2011), Regional moment tensor of the 2009 L'Aquila earthquake sequence, *Bull. Seismol. Soc. Am.*, *101*(3), 975–993.

INGV Working Group "GPS Geodesy (GPS data and data analysis center)" (2016), Preliminary co-seismic displacements for the August 24, 2016 M_L6.0, Amatrice (Central Italy) earthquake from the analysis of continuous GPS stations, doi:10.5281/zenodo.61355.

INGV-ReLUIS Working Group (2016), Preliminary study of Rieti earthquake ground motion data V5, 1–87, doi:10.13140/RG.2.2.27933.92641/1. [Available at http://www.reluis.it].

Lavecchia, G., F. Ferrarini, F. Brozzetti, R. De Nardis, P. Boncio, and L. Chiaraluce (2012), From surface geology to aftershock analysis: Constraints on the geometry of the L'Aquila 2009 seismogenic fault system, *Ital. J. Geosci. (Boll. Soc. Geol. Ital.)*, *131*(3), 330–347, doi:10.3301/IJG.2012.24.

Rovida, A., Locati M., Camassi R., Lolli B., and Gasperini P. (Eds.) (2016), CPTI15, the 2015 version of the Parametric Catalogue of Italian Earthquakes, Istituto Nazionale di Geofisica e Vulcanologia, doi:10.6092/INGV.IT-CPTI15.

Saikia, C. (1994), Modified frequency-wave number algorithm for regional seismograms using Filon's quadrature; modelling of Lg waves in eastern North America, *Geophys. J. Int.*, *118*, 142–158.

Scognamiglio, L., E. Tinti, A. Michelini, D. S. Dreger, A. Cirella, M. Cocco, S. Mazza, and A. Piatanesi (2010), Fast determination of moment tensors and rupture History: What has been learned from the 6 April 2009 L'Aquila earthquake sequence, *Seismol. Res. Lett.*, *81*(6), 892–906, doi:10.1785/gssrl.81.6.892.

Stucchi, M., et al. (2011), Seismic hazard assessment (2003–2009) for the Italian building code, *Bull. Seismol. Soc. Am.*, *101*(4), 1885–1911, doi:10.1785/0120100130.

Wang, C. Y., and R. B. Herrmann (1980), A numerical study of *P*-, *SV*-, and *SH*-wave generation in a plane layered medium, *Bull. Seismol. Soc. Am.*, *70*(4), 1015–1036.